Photodissociation dynamics of weakly bound HeH_2^+ in intense light fields

Tamás Szidarovszky* and Kaoru Yamanouchi
Department of Chemistry, School of Science, The University of Tokyo, Tokyo, Japan
(Received 5 September 2016; published 6 December 2016)

Photoinduced dynamics of a weakly bound triatomic molecule HeH_2^+ exposed to electromagnetic radiation is investigated by time-dependent quantum wave-packet propagation. Adopting a two-dimensional linear H-H-He model, the three lowest-lying potential energy surfaces (PESs) and corresponding dipole moment surfaces are constructed. One of the two characteristic excited PESs of HeH_2^+ leads to the charge-transfer reaction $H_2^+ + He \rightarrow H_2 + He^+$ and the other corresponds to the first excited state of H_2^+ perturbed by the presence of He. When HeH_2^+ is exposed to a femtosecond intense ultraviolet light pulse ($I = 4 \times 10^{14}$ W cm^{-2}, $\lambda = 400$ nm), both of the two excited PESs are found to be coupled with the light field and a variety of reaction pathways become opened so that HeH, HeH^+, H_2, H_2^+, H, H^+, He, and He^+ are produced. Simulations also show that the anharmonic coupling between the two stretching vibrational modes in HeH_2^+ leads to the stabilization of the H_2^+ moiety against the decomposition into $H + H^+$ compared with bare H_2^+. The theoretical findings of the formation of HeH^+ composed of the most abundant elements in the universe are also discussed in view of the theoretical modeling of the chemical reactions proceeding in the primordial gas and in the interstellar medium.

DOI: 10.1103/PhysRevA.94.063405

I. INTRODUCTION

A detailed understanding of the interaction of molecules and strong electromagnetic fields is the basis for the interpretation of laser-induced and laser-controlled photochemical reactions. The dynamics of the simplest molecular systems, H_2^+ and its isotopologs, in intense laser fields have been one of the most attractive issues in theoretical and experimental studies (see, for example, Refs. [1–7] and references therein). Despite the simplicity of H_2^+, characteristic light-dressed dynamics induced by a laser field have been discovered through its study, such as one-photon crossing, three-photon crossing followed by two-photon dissociation, bond softening, bond hardening, zero-photon dissociation, enhanced ionization, and charge-resonance enhanced ionization. In its electronic ground state, the weakly bound HeH_2^+ molecule can be viewed as an H_2^+ molecule perturbed by He. It is therefore interesting to investigate the light-induced processes of HeH_2^+, as they reveal how the characteristic dynamics of H_2^+ in a laser field is influenced by the addition of He as the smallest perturber to form a weakly bound complex with H_2^+. Among the possible photoinduced processes of HeH_2^+, those induced by an intense light field are of special interest because such an intense light field could induce strong coupling among the electronic states, leading to intramolecular charge transfer followed by large-scale rearrangement of nuclei within HeH_2^+. Unexpectedly, as introduced in the present report, we found that the addition of He to H_2^+ drastically changes the photoinduced processes of H_2^+. For example, the chemical bond rearrangement process yielding HeH^+ and the light-induced charge-transfer process yielding neutral H_2 were identified.

Such photoinduced processes can be relevant not only in understanding molecular dynamics proceeding in an intense laser field, but also in understanding elementary chemical reaction processes occurring in outer space. HeH_2^+ is composed of the two of the most abundant elements in the universe and should have played an important role in the chemical reactions in the primordial gas [8] and in the interstellar medium (ISM) [9,10], together with hydrogen atoms, helium atoms, and their ionized forms. Indeed, HeH_2^+ can be produced instantaneously in the collisions of $H_2^+ + He$, $H_2 + He^+$, and $HHe^+ + H$, and it was considered that $HeH^+ + H \rightarrow He + H_2^+$ was the first bimolecular chemical reaction in the universe [11], possibly contributing to the cooling processes of the primordial gas [12].

For astrophysically relevant molecules, not only their field-free properties but also their dynamical properties induced by a light field are important. In the cooling processes of the primordial universe, the rovibronic excitation of such small molecules of the first generation by radiation played an essential role [12]. Also, light-induced processes can occur when molecules are exposed to cosmic radiation in the ISM, leading to a variety of chemical reactions [9,10]. For example, photoionization of H_2 in the ISM is the first step in the creation of triatomic H_3^+, which then becomes a precursor species leading to the formation of organic molecules and water through a chain of chemical reactions [13]. It is possible that the triatomic HeH_2^+, being a stable molecule possibly existing in the ISM [14], serves as a precursor species for the formation of H,H^+, He, He^+, H_2, H_2^+, HeH, or HeH^+. Outer space is filled with electromagnetic radiation covering wide wavelength and intensity ranges, such as the cosmic microwave background radiation [15], the blackbody radiation of stars peaking in the infrared and the visible range, the ultraviolet light emitted by stars or quasars [16,17], and the high-intensity radiation in the vicinity of white dwarfs or neutron stars [16].

Therefore, although our investigations on the light-induced processes of HeH_2^+ are carried out in the context of molecular interactions with ultrafast intense light fields, the identified processes can also be elementary photoinduced reactions proceeding in the ISM.

II. POTENTIAL ENERGY SURFACES

The field-free HeH_2^+ molecule has already been investigated previously in experimental studies, either as

*tamas821@gmail.com

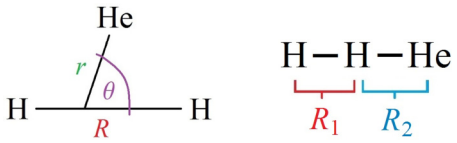

FIG. 1. Visual presentation of the Jacobi coordinates (left panel) and the $R_1 = r$(H–H) and $R_2 = r$(H–He) stretching coordinates (right panel).

the collisional complex in the collisions of $He^+ + H_2$ and $He + H_2^+$ [18–20], or by ion beam microwave spectroscopy [21]. Also, its PESs [22–28], dipole moment surfaces (DMS) [29,30], (ro)vibrational levels [14,26], and transition energies [29,30] have been calculated for facilitating its spectroscopic detection in outer space [14,29,30], as well as for investigating the collisional processes of $H_2^+ + He$ or $H_2 + He^+$ [23–25,31,32]. Based on the PES of the electronic ground state of HeH_2^+ obtained by Palmieri *et al.* [24], which may be among the most accurate to date [25], HeH_2^+ has two equivalent minima at the linear configurations, corresponding to "H-H-He^+" and "He-H-H^+". In terms of the Jacobi coordinates [33], which are shown in the left panel of Fig. 1, the minima are located near a H–H distance of $R = 2.09$ bohr and H_2^+–He distance of $r = 2.96$ bohr, with $\theta = 0$ or π.

The first spectroscopic dissociation energy D_0 for $HeH_2^+ \rightarrow H_2^+ + He$ is as small as around $D_0 = D_e - E_{ZPVE}^{H_2He^+} + E_{ZPVE}^{H_2^+} = (2740 - 2110 + 1150)\,cm^{-1} = 1780 cm^{-1}$, showing that HeH_2^+ is a weakly bound complex [24,25]. In the above equation, $D_e, E_{ZPVE}^{H_2He^+}$, and $E_{ZPVE}^{H_2^+}$ are the potential depth, the zero point vibrational energy (ZPVE) of HeH_2^+, and the ZPVE of H_2^+, respectively.

In the present report, we investigate the photodissociation and nuclear dynamics of HeH_2^+ induced by an irradiation of a high-intensity femtosecond light pulse. In order to discuss such nuclear dynamics proceeding in an intense light field with an intensity comparable to that of the Coulombic field in atoms and molecules, a number of electronically excited states need to be included in the calculations because they are coupled with each other by the external light field. In addition, when nuclei move in a wide range on the PESs, as in the cases of large-amplitude vibration and photodissociation, global representations of the PESs and the corresponding transition DMSs need to be prepared. Figure 2 shows the three lowest-lying adiabatic PESs of the linear HeH_2^+ molecule as a function of the H-H and H-He distances, obtained in the present study on a FCI/aug-cc-pVTZ level [34–36] using the MRCC program suite [37]. Asymptotic atom-diatom dissociation products are also indicated. The resultant PES of the ground electronic state is in good agreement with previous studies [23,24]. Indeed, the relative energy with respect to the PES minimum for the geometries along the two dissociation pathways $HeH_2^+ \rightarrow H_2^+ + He$ and $HeH_2^+ \rightarrow HeH^+ + H$ agree to better than $20\,cm^{-1}$ with those obtained from the PES of Ref. [24].

In the large H-He internuclear distance regions of HeH_2^+ in Fig. 2, $r(H - He) > 3$ bohr, the $^2\Sigma_g^+$ and $^2\Sigma_u^+$ potential energy curves (PECs) of H_2^+ can be seen on the two-dimensional PESs along the H-H internuclear distance axis, representing H_2^+ in the vicinity of He. Henceforth the corresponding two states are denoted as $[H_2^+(^2\Sigma_g^+)—He]$ and $[H_2^+(^2\Sigma_u^+)—He]$. Interestingly, the $^1\Sigma_g^+$ ground-state PEC of H_2 shifted by the ionization potential of He, representing a charge transfer state, henceforth denoted as $[H_2(^1\Sigma_g^+)—He^+]$, crosses the PEC of $[H_2^+(^2\Sigma_u^+)—He]$ at the H–H distance of around 2 bohr. For the shorter H–He distance regions, the seam of the intersection develops into an avoided crossing.

In order to account for the nonadiabatic couplings in the vicinity of the conical intersection as well as of the avoided crossing [38], we transformed the two excited electronic states into the diabatic basis from the adiabatic basis by a unitary transformation [39] by which the two-by-two dipole moment matrices corresponding to the two excited states are diagonalized. It was found that the magnitude of the off-diagonal potential matrix elements, representing the nonadiabatic couplings in the diabatic representation, are negligibly small except in the H–H distance region of around 1.6–2.8 bohr. The largest magnitude of the nonadiabatic couplings is around $1200\,cm^{-1}$ near 2 bohr.

The presence of the PES corresponding to the charge-transfer state $[H_2(^1\Sigma_g^+)—He^+]$, through which the charge-transfer reaction $H_2^+ + He \rightarrow H_2 + He^+$ could proceed, suggests that a variety of possible dissociation products, H,H^+, He, He^+, H_2, H_2^+, HeH, and HeH^+, can be formed once $[H_2^+(^2\Sigma_g^+)—He]$ is excited by the photoirradiation. Because the vertical excitation energies from $[H_2^+(^2\Sigma_g^+)—He]$ to $[H_2^+(^2\Sigma_u^+)—He]$ and to $[H_2(^1\Sigma_g^+)—He^+]$ are around $97\,000\,cm^{-1}$ and $114\,000\,cm^{-1}$, respectively, vacuum ultraviolet light whose wavelength is shorter than 100 nm is required for the preparation of these two electronically excited states by single photon absorption. When adopting longer wavelength light, its field intensity needs to be sufficiently strong so that these two electronically excited states are prepared through multiphoton absorption.

III. WAVE-PACKET PROPAGATION

To investigate the time-dependent nuclear dynamics of HeH_2^+ in intense light fields, a spatially aligned linear model was adopted in which the molecule has a linear H-H-He structure whose molecular axis is parallel to the light polarization direction. Experimentally, this situation in which the H-H-He molecular axis becomes parallel to the laser polarization direction can be realized by the laser-induced alignment of HeH_2^+ with an additional aligning pulse, as detailed in the Appendix A.

In the simulation of the motion of the nuclear wave packet, the three lowest-lying PESs of HeH_2^+ (see Fig. 2) were considered, and the dipole coupling is treated as a coupling between a quantum-mechanically treated molecule and a classically treated electromagnetic field (Gaussian-shaped light pulse with $\lambda = 400$ nm wavelength, $I = 4 \times 10^{14}$ W cm^{-2} intensity, and $\Gamma = 11.4$ fs FWHM of the electric field). In order to test the convergence of our results with respect to the number of electronic states, we conducted calculations including three additional higher lying excited-state PESs, and found that the light-induced dynamics did not exhibit noticeable change, i.e., the additional PESs were only negligibly populated during the light matter interaction because of their low transition dipoles.

Using two stretching coordinates, $R_1 = r$(H–H) and $R_2 = r$(H–He) (see right panel of Fig. 1), the reduced

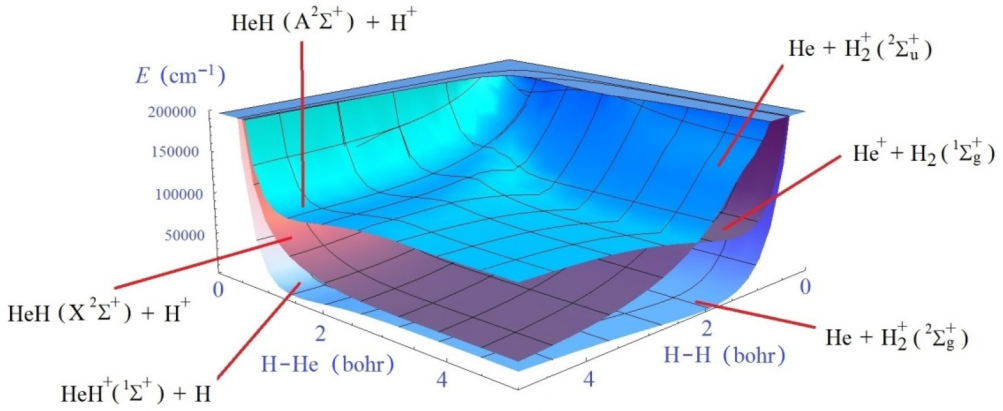

FIG. 2. Three lowest-lying adiabatic potential energy surfaces of the linear $(H–H–He)^+$ molecule as a function of the H–H and H–He distances. Asymptotic atom-diatom dissociation products are also indicated.

dimensional nuclear Hamiltonian can be expressed in atomic units as [40]

$$\hat{\mathbf{H}}^{\mathrm{2D,valence}}(R_1,R_2,t) = \mathbf{E}_3 \otimes \left(-\frac{1}{m_{\mathrm{H}}}\frac{\partial^2}{\partial R_1^2} + \frac{1}{m_{\mathrm{H}}}\frac{\partial}{\partial R_1}\frac{\partial}{\partial R_2} - \frac{m_{\mathrm{H}}+m_{\mathrm{He}}}{2m_{\mathrm{H}}m_{\mathrm{He}}}\frac{\partial^2}{\partial R_2^2}\right) + \begin{bmatrix} V_{11}(R_1,R_2) & 0 & 0 \\ 0 & V_{22}(R_1,R_2) & V_{23}(R_1,R_2) \\ 0 & V_{32}(R_1,R_2) & V_{33}(R_1,R_2) \end{bmatrix} - \varepsilon(t)\begin{bmatrix} \mu_{11}(R_1,R_2) & \mu_{12}(R_1,R_2) & \mu_{13}(R_1,R_2) \\ \mu_{21}(R_1,R_2) & \mu_{22}(R_1,R_2) & 0 \\ \mu_{31}(R_1,R_2) & 0 & \mu_{33}(R_1,R_2) \end{bmatrix}, \quad (1)$$

where $\mathbf{E}_3$ is a 3×3 unit matrix, $\varepsilon(t)$ is the light field amplitude, and V_{ij} and μ_{ij} respectively denote the potential energy matrix elements and transition dipole moment matrix elements in the diabatic electronic basis. As the nuclear masses of H and He, $m_{\mathrm{H}} = 1.007\,276\,47$ u and $m_{\mathrm{He}} = 4.002\,347\,55$ u are adopted. An alternative expression $\hat{\mathbf{H}}^{\mathrm{2D,Jacobi}}(R,r,t)$ for the Hamiltonian can easily be obtained in Jacobi coordinates by using the chain rule, and the relations $R_1 = R$ and $R_2 = r - 0.5R$. Although converged results are independent of the coordinate system used, $\hat{\mathbf{H}}^{\mathrm{2D,Jacobi}}(R,r,t)$ is more convenient for numerical simulations, since in Jacobi coordinates the kinetic coupling term present in Eq. (1) vanishes; thus vibrational couplings are expressed solely by the potential.

The matrix representation of $\hat{\mathbf{H}}^{\mathrm{2D,Jacobi}}(R,r,t)$ was constructed using a direct product *discrete variable representation* (DVR) basis [41], and the time propagation of the initial wave packet was performed using the "*absorbing boundary condition time propagator*" of Ref. [42], as detailed in Appendix B. The initial wave packet was chosen to be in the vibrational ground state of HeH_2^+. In order to see the relative yields of the fragments produced from the different dissociation pathways as a function of time, the amount of the probability density absorbed by the time propagator at the different asymptotic regions of the PESs were calculated at different times and are presented in Fig. 3. Snapshots of the nuclear wave packet on the three different PESs at different times are shown in Fig. 4.

In order to examine the stabilization of H_2^+ when He is attached, the nuclear dynamics of the spatially fixed H_2^+ exposed to the same light field as in the case of HeH_2^+ was also simulated by taking into account its two lowest electronic states. The temporal change of the norms of the wave packet for H_2^+ and HeH_2^+ is presented in Fig. 6(a). As will be described in the next section, Fig. 6(a) shows that by the presence of He the stabilization of H_2^+ is achieved.

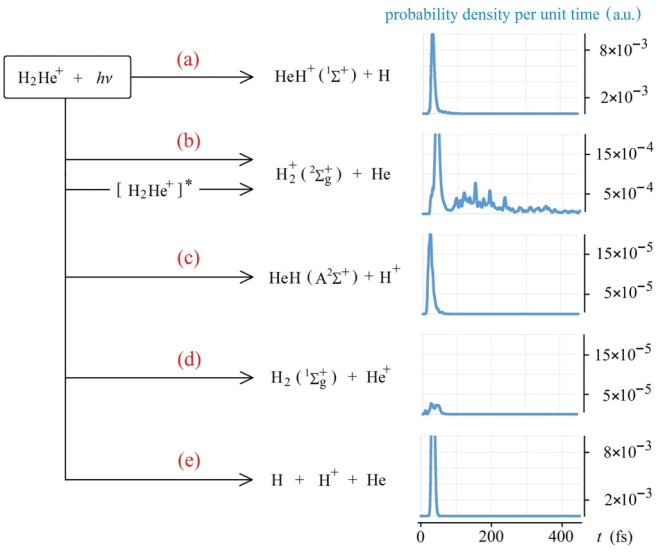

FIG. 3. Different HeH_2^+ photodissociation channels and product yields, which are defined as the probability density absorbed at the asymptotic regions of the coordinate space, as a function of time, when the molecule is exposed to a Gaussian-shaped light pulse ($\lambda = 400$ nm, $I = 4 \times 10^{14}$ W cm^{-2}, $\Gamma = 11.4$ fs FWHM of the electric field).

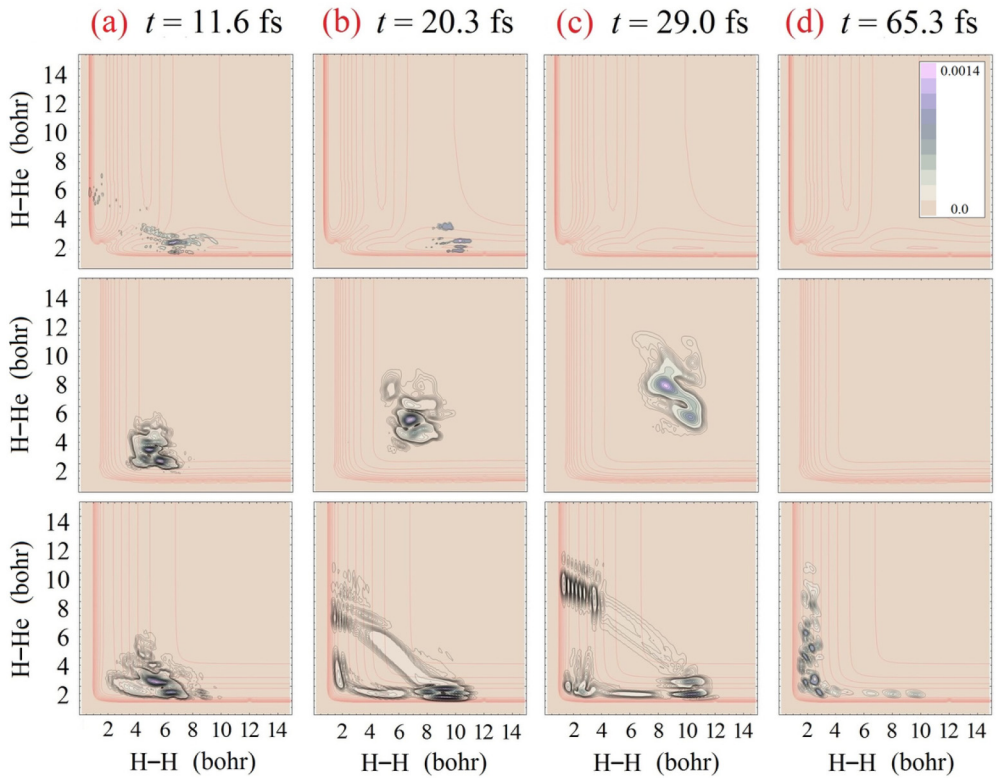

FIG. 4. Nuclear wave-packet components on the three potential energy surfaces at different times. Contour lines of the respective potential energy surfaces are indicated in red.

IV. PHOTODISSOCIATION CHANNELS

Figure 5 shows the temporal evolution of the populations on the three PESs. It can be seen in Fig. 5 that the populations rapidly oscillate during the light-matter interaction, and also show interference-type patterns arising from the coherent population transfer between the different PESs. This oscillation of the populations, which is absent in the weak-field single-photon absorption processes, naturally plays a considerable role in the final product yields. It is also seen in Fig 5 that although the two excited electronic states have comparable transition dipoles, most of the transferred population ends up in the first excited $[H_2{}^+(^2\Sigma_u^+)$—He] state. This is most probably due to its lower vertical excitation energy.

By comparing the norms of the wave packets for $H_2{}^+$ and $HeH_2{}^+$ as a function of time, as presented in Fig. 6(a), it was found that not all of the $HeH_2{}^+$ undergoes dissociation but about 90%, which is less than the 100% complete dissociation of bare $H_2{}^+$.

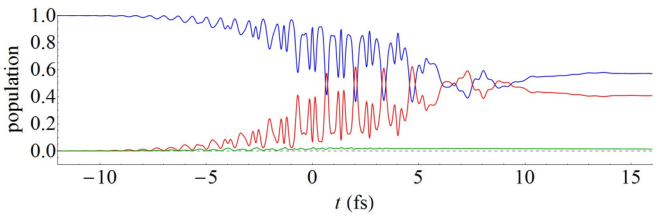

FIG. 5. Temporal evolution of the populations on the (blue) ground electronic state, (red) first excited $[H_2{}^+(^2\Sigma_u^+)$—He] electronic state, and (green) second excited $[H_2(^1\Sigma_g^+)$—$He^+]$ electronic state. The external field amplitude reaches its peak at 0 fs.

Among this 90%, there are two different groups of dissociation pathways, that is, (i) detachment of He or He^+ from the $H_2{}^+$ or H_2 moiety, respectively, (27.7%) and (ii) H–H bond breaking (62.3%), leading to the breakups $HHe^+ + H$ and $HHe + H^+$ or the three-body decomposition producing H, H^+, and He. The stabilization effect associated with the attachment of He originates both from the modification of the electronic structure in the $H_2{}^+$ moiety, as seen in the differences in the H–H PECs at different H–He distances in Fig. 2, and from the vibrational couplings between the H–He and H–H stretching motions.

As can be seen from Figs. 3 and 6(a), fast photodissociation processes (83.9% of the total yield) of $HeH_2{}^+$ start proceeding in a few femtoseconds, and the corresponding wave-packet portions are eventually absorbed at the respective asymptotic regions of the PESs around 30–50 fs after the light pulse amplitude reaches its peak ($t = 0$ fs).

Additionally, a slow decaying process is observed (16.1% of the total yield), for which the absorbance of the wave packet starts appearing roughly 80 fs after the light pulse reaches its peak, but continues over 300–400 fs. Hereafter, the fast and slow processes will refer to the time scales of around 30–50 fs and 300–400 fs, respectively.

Within the fast dissociation pathways, the three most dominant channels are (i) $HeH_2{}^+ \rightarrow HeH^+(X\,^1\Sigma^+) + H$ (35.3%), in which the H–H bond is broken on the ground-state PES; (ii) $HeH_2{}^+ \rightarrow H_2{}^+ + He$ (17.3%), in which the H-He bond is broken on the ground-state PES; and (iii) $HeH_2{}^+ \rightarrow$

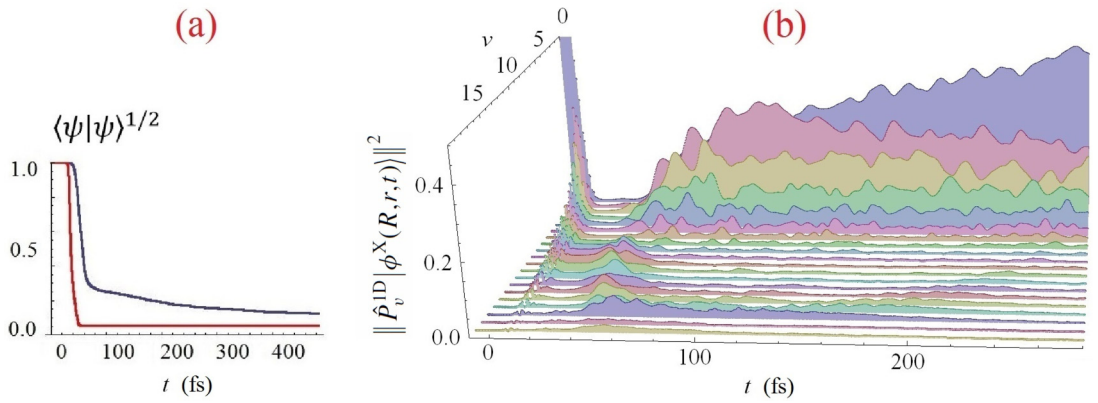

FIG. 6. (a) Temporal evolution of the norm of the wave packet of $H_2{}^+$ (red) and that of $HeH_2{}^+$ (blue), and (b) distributions of the norms of wave-packet projections onto the vibrational eigenstates of $H_2{}^+$ as a function of time, as computed by Eq. (2).

$H^+ + H + He$ (46.2%), in which the H–H bond is broken on the $[H_2{}^+(^2\Sigma_u^+)$—He] PES, as seen in panels (a), (b), and (e) of Fig. 3, respectively. In the reaction $HeH_2{}^+ \rightarrow HeH^+(X^1\Sigma^+) + H$, the weak bonding between He and H_2 in $HeH_2{}^+$ is replaced by a stronger H-He bond in HeH^+, representing a bond rearrangement pathway.

An interesting finding is the existence of the reaction pathway $HeH_2{}^+ \rightarrow HHe\,(A^2\Sigma^+) + H^+$, shown in Fig. 3(c). Through this fourth dominant (1.0%) fast process, the first electronically excited state $A^2\Sigma^+$ of neutral HeH is produced. It should be noted that the interatomic potential of HeH in the electronic ground $X^2\Sigma^+$ state is repulsive, while that in the first electronically excited $A^2\Sigma^+$ state forms a bound well whose dissociation energy is around 20 700 cm^{-1} [43]. This means that population inversion can be realized in the produced HeH molecules, suggesting the possibility of lasing to take place at around 300 nm (XUV). The fifth fast process with the very small yield (0.2%) is the reaction pathway, $HeH_2{}^+ \rightarrow H_2 + He^+$, which can be categorized into a photoinduced charge-transfer process occurring between $H_2{}^+$ and He within the $HeH_2{}^+$ complex.

The slow decay process shown in Fig. 3(b) is the breaking of the weak intermolecular H–He bond, $HeH_2{}^+ \rightarrow H_2{}^+ + He$, proceeding as a result of intramolecular energy redistribution among the vibrational modes as will be discussed below.

The time-dependent wave-packet dynamics can be interpreted by the superposition of time-independent stationary states of the field-free system. The fast dissociation processes occurring within a few tens of femtoseconds can be ascribed to the rapid decay of the dissociative continuum states of the respective dissociation channels populated through the interaction with the light field. On the other hand, the slow decaying process with the half-life of several hundreds of femtoseconds can be ascribed to the decay of the metastable Feshbach-resonance [44] states storing the energy in nondissociative vibrational degrees of freedom. As will be shown below, in the case of $HeH_2{}^+$, the excess energy is stored in the H–H stretching mode, along which the D_0 dissociation energy is $D_0 = D_e - E_{ZPVE}^{H_2He^+} + E_{ZPVE}^{HeH^+} = (8775 - 2110 + 1575)\ cm^{-1} = 8240\ cm^{-1}$ [24,25], which is considerably larger than the dissociation energy of 1780 cm^{-1} along the He–H stretching mode.

We conclude this section by presenting dissociation yields for weak-field single-photon photodissociation. Since the vertical excitation energy for the two excited-state PESs differ by about 17 000 cm^{-1}, a one-photon absorption process could take place by promoting the wave function to either the $[H_2{}^+(^2\Sigma_u^+)$—He] or the $[H_2(^1\Sigma_g^+)$—$He^+]$ PES. Wave-packet propagation simulations were carried out for these two cases with the initial wave packets obtained as the vibrational ground state of $HeH_2{}^+$ on the electronic ground state, multiplied by the transition dipole corresponding to the respective excited electronic state. In the case of photoexcitation to the $[H_2{}^+(^2\Sigma_u^+)$—He] PES, the relative dissociation yields are 99.83% for the $HeH_2{}^+ \rightarrow H^+ + H + He$ breakup, 0.14% for the $HeH_2{}^+ \rightarrow H_2 + He^+$ breakup, and 0.03% for the $HeH_2{}^+ \rightarrow HHe\,(A^2\Sigma^+) + H^+$ breakup, the latter two being a result of nonadiabatic population transfer. When the initial wave packet is localized on the $[H_2(^1\Sigma_g^+)$—$He^+]$ PES, the relative dissociation yields for the same channels are 1.33%, 5.09%, and 93.58%, respectively. Based on these values and their comparison with the strong-field case, it can be concluded that the nonadiabatic coupling primarily promotes population transfer from the $[H_2(^1\Sigma_g^+)$—$He^+]$ PES to the $[H_2{}^+(^2\Sigma_u^+)$—He] PES, and that the production of HHe $(A^2\Sigma^+)$ with respect to the production of H_2 is strongly promoted in the strong-field case.

V. NUCLEAR DYNAMICS

In order to understand the vibrational dynamics of the system, we monitored the wave-packet component in the ground electronic state $|\phi^X(R,r,t)\rangle$ by computing the Euclidian norm [45] of its projection onto the different vibrational eigenstates of the $H_2{}^+$ molecule, denoted by $|\psi_v^{1D}(R)\rangle$, where v stands for the vibrational quantum number. Based on the DVR basis expansions, $|\phi^X(R,r,t)\rangle = \sum_{i=1}^{N_1}\sum_{j=1}^{N_2} C_{ij}^X(t)|\varphi_i^{DVR}(R)\rangle \otimes |\varphi_j^{DVR}(r)\rangle$, $|\psi_v^{1D}(R)\rangle = \sum_{k=1}^{N_1} c_k^v|\varphi_k^{DVR}(R)\rangle$, and the projector onto the specific eigenstates, $\hat{P}_v^{1D} = |\psi_v^{1D}\rangle\langle\psi_v^{1D}|$, the squared norm of the wave-packet projection is

$$\left\|\hat{P}_v^{1D}|\phi^X(R,r,t)\rangle\right\|^2 = \sum_{j=1}^{N_2}\left|\sum_{i=1}^{N_1} C_{ij}^X(t)c_i^{v*}\right|^2. \qquad (2)$$

Figure 6(b) shows the norms of the wave-packet projections onto H_2^+ vibrational eigenstates computed by Eq. (2) as a function of time. It can be seen that, prior to its excitation by the light field, the H_2^+ moiety is almost exclusively in its ground vibrational state. As soon as after the light field is introduced, the vibrational eigenstates of H_2^+ are strongly mixed as seen in Fig. 6(b). After the light field disappears, the populations in the excited vibrational eigenstates of H_2^+ are gradually transferred to the lower-lying vibrational eigenstates of H_2^+ in the course of the wave-packet propagation. This population transfer can be related to the slow decaying process of $HeH_2^+ \rightarrow H_2^+ + He$ as follows: when the H-H stretching vibration in the H_2^+ moiety is excited, the energy stored in the H–H stretching motion of HeH_2^+ is transferred to the H–He stretching vibration through the kinetic coupling [Eq. (1)] and the anharmonic couplings between the two degrees of freedom, leading eventually to the breaking of the weaker H–He bond. From the time-independent viewpoint discussed in the previous section, i.e., the wave packet being a superposition of bound and metastable stationary states, the temporal decrease of the H–H excitation can be explained by the metastable states with higher H–H excitation being shorter lived and depopulating more rapidly.

Another interesting feature of the wave-packet dynamics can be seen in panels (a), (b), and (c) of Fig. 4. Around $t = 11-12$ fs, the wave-packet portion located on the ground electronic state near r(H–H) = 6 bohr and r(H–He) = 2 bohr bifurcates, one part leading to the dissociation into $HeH_2^+ \rightarrow HHe^+ + H$, while the other part moves along the antisymmetric stretching mode, as shown in panels (b) and (c) of Fig. 4. This latter component eventually leads to the dissociation $HeH_2^+ \rightarrow H_2^+ + He$, producing vibrationally highly excited H_2^+, as can be seen from the nodal structure in Fig. 4(c) around r(H–H) = 2 bohr and r(H–He) = 9 bohr. When using the $R_1 = r$(H–H) and $R_2 = r$(H–He) coordinates to express the ground-state PES, its form suggests that the asymmetric stretching-type motion of the wave packet is not likely to be induced by the potential, indicating that it is rather originated from the kinetic coupling in Eq. (1).

VI. SUMMARY AND CONCLUSIONS

A weakly bound atom-diatom complex, HeH_2^+, exposed to a femtosecond light pulse was investigated. The three lowest-lying PESs and corresponding transition DMSs were computed globally for linear geometries, that is, for H–H and He–H distances up to 10 bohr. It was found that the PES corresponding to the charge-transfer $H_2^+ + He \rightarrow H_2 + He^+$ contributes to the photodissociation processes of HeH_2^+ through the light-induced reactions $HeH_2^+ \rightarrow HeH + H^+$ and $HeH_2^+ \rightarrow H_2 + He^+$. The two-dimensional, time-dependent quantum-wave-packet propagations showed that the linear HeH_2^+, when exposed to a femtosecond intense light pulse ($I = 4 \times 10^{14}$ W cm^{-2}, $\lambda = 400$ nm, polarization direction parallel to the H-H-He axis), undergoes rich photodissociation dynamics. The results obtained from the simulations are summarized as follows: (i) a variety of photofragments such as HeH, HeH^+, H_2, H_2^+, H,H^+, He, and He^+ are produced from the three PESs; (ii) after the rapid dissociation processes occurring within 30–50 fs, the slow decaying process lasts until around 300–400 fs on the ground-state PES along the H–He coordinate via the intramolecular vibrational energy redistribution (IVR) from the vibrationally excited moiety of H_2; (iii) the couplings among the vibrational degrees of freedom stabilize both the H_2^+ moiety and the entire HeH_2^+ molecule, thus significantly affect the dissociation product yields, and (iv) the dissociation probability of the H_2 moiety in HeH_2^+ is smaller by 38% than that of bare H_2^+ under the light field conditions adopted in the present report. The stabilization effect of He originates both from the anharmonic vibrational couplings between the H–He and H–H stretching modes, and from the change induced by He in the electronic structure around the H_2^+ moiety, as can be seen in the differences in the H–H potential energy curves at different H–He distances in Fig. 2.

As long as the electronic ground state of HeH_2^+ is concerned, it can be regarded as H_2^+ perturbed by He through the weak $H_2^+ -$ He interaction. However, in the presence of an intense light field, He becomes an active reactant influencing the vibrational dynamics of H_2^+ as well as leading to the chemical bond breaking in H_2^+ to form diatomic fragments of HeH and HeH^+. It is possible that the formation of the weakly bound complex of HeH_2^+ in the outer space played a key role in cooling the primordial gas in the early-stage universe through the formation of HeH^+.

ACKNOWLEDGMENTS

The work described received support from the Grant-in-Aid (Tokubetsu Kenkyuin Shorei-hi) Scientific Research Fund of JSPS (Japan Society for the Promotion of Science), Project No. 26-04333, and the JSPS KAKENHI Grant No. 15H05696.

APPENDIX A: ADIABATIC ALIGNMENT OF HeH_2^+

Through the interaction with a medium intensity off-resonant laser field, molecules can undergo adiabatic spatial alignment [46]. In this Appendix the laser-induced alignment of HeH_2^+ is investigated by computing the eigenstates of the Hamiltonian

$$\hat{H} = \hat{H}_0 - 1/4\boldsymbol{\varepsilon}(\boldsymbol{\alpha}\boldsymbol{\varepsilon}), \tag{A1}$$

where $\hat{H}_0$ is the field-free rovibrational Hamiltonian and $-1/4\boldsymbol{\varepsilon}(\boldsymbol{\alpha}\boldsymbol{\varepsilon})$ is the time-averaged induced dipole interaction with the external aligning field. The matrix representation of $\hat{H}$ was constructed in the full set of bound rovibrational eigenstates of the field-free HeH_2^+ molecule, obtained by full-dimensional variational rovibrational computations using the PES of Ref. [25] and the D^{2}FOPI program suite [47]. Computational details on the calculation of the rovibrational states, the matrix elements of $\hat{H}$, and the construction of the $\boldsymbol{\alpha}$ polarizability surfaces are detailed below.

By inspecting the lowest-energy eigenstates of $\hat{H}$, it was found that significant adiabatic spatial alignment of HeH_2^+ can be achieved. For example, by applying an off-resonant laser field whose intensity is $I = 2 \times 10^{13}$ W cm^{-2}, the extent of the alignment was found to be $\langle\cos^2(\phi)\rangle \cong 0.84$ and $\langle\cos^2(\theta)\rangle \cong 0.91$, where $\langle . \rangle$ is the expectation value for the rovibrational wave packet, ϕ is the angle between the molecule-fixed and laboratory-fixed Cartesian z axes, and θ is the Jacobian angle. The aligned state was found to be a

superposition of purely rotationally excited eigenstates, that is, no vibrational excitation occurs during the alignment. Furthermore, by computing the structural parameters of the aligned state, it was found that the geometrical structure of the aligned molecule is essentially the same as the field-free ground rovibrational state taking the linear geometry.

Therefore, prior to its photodissociation, spatial alignment of the linear triatomic molecule, HeH_2^+, can be achieved with an additional aligning laser pulse, without distorting the linear geometrical structure. As was explained in the previous studies [48–50], the above results rationalize to investigate the time-dependent photodissociation processes of HeH_2^+ induced by an intense femtosecond laser pulse in a reduced dimensional model by assuming that the molecule has a linear H-H-He structure whose molecular axis is parallel to the light polarization direction.

For computing the field-free, bound rovibrational eigenstates of HeH_2^+ supported by the PES of De Fazio *et al.* [25], full-dimensional variational computations in Jacobi coordinates were carried out with the D^{2}FOPI program suite, exploiting the C_{2v}(M) molecular symmetry [51] of the system, as described in Ref. [52]. The D^{2}FOPI program solves the triatomic time-independent rovibrational Schrödinger equation using a mixed DVR and *finite basis represenation* (FBR) [41] for representing the vibrational degrees of freedom in an *orthogonal coordinate system*, applying a *direct product basis* and an *iterative eigensolver*. The rotational basis functions utilized in D^{2}FOPI are symmetry adopted Wigner matrices. For each irreducible representation of the C_{2v}(M) molecular symmetry group, the calculations employed a complete set of rotational basis functions whose size depends on the given value of the J rotational quantum number, 20 and 60 potential-optimized (PO) spherical-DVR basis functions [47] along the R and r coordinates, respectively, and 15 associated Legendre funcions along the θ coordinate. The coordinate ranges used were $R \in (0,4)$ bohr and $r \in (0,15)$ bohr, and the nuclear masses $m_{\mathrm{H}} = 1.007\,276\,47$ u and $m_{\mathrm{He}} = 4.002\,347\,55$ u were employed.

The full-dimensional rovibrational wave functions of the field-free system are obtained from the variational rovibrational calculations as expansions

$$\Psi^{JMn}(R,r,\theta,\varphi,\vartheta,\chi) = \sqrt{\frac{2J+1}{8\pi^2}} \sum_{K,v} C_{Kv}^{Jn} \psi_v(R,r,\theta) D_{MK}^{J*}(\varphi,\vartheta,\chi), \quad \text{(A2)}$$

where C_{Kv}^{Jn} are expansion coefficients, J is the rotational quantum number, K is the projection of the rotational angular momentum onto the body-fixed z axis, M is the projection of the rotational angular momentum onto the space fixed z axis, n is "all other" quantum numbers, $\psi_v(R,r,\theta)$ is the vth vibrational basis function, and $D_{MK}^{J}(\varphi,\vartheta,\chi)$ is a Wigner matrix [53]. φ,ϑ, and χ are the standard three Euler angles describing the orientation of the body-fixed (BF) coordinate frame with respect to the laboratory frame (LF).

The matrix elements of the Hamiltonian of Eq. (A1) in the basis of field-free states $|\Psi^{JMn}\rangle$ were calculated by expressing the Cartesian components of the polarizability tensor in the so-called spherical-basis [53] representation, for which the transformation formulas are $\alpha^{(0)} = -\frac{1}{\sqrt{3}}(\alpha_{11}+\alpha_{22}+\alpha_{33}) = -\frac{1}{\sqrt{3}}\mathrm{Tr}[\alpha]$, $\alpha^{(2,\pm2)} = \frac{1}{2}[\alpha_{11}-\alpha_{22} \pm i(\alpha_{12}+\alpha_{21})]$, $\alpha^{(2,\pm1)} = \frac{1}{2}[\mp(\alpha_{13}+\alpha_{31}) - i(\alpha_{23}+\alpha_{32})]$, and $\alpha^{(2,0)} = \frac{1}{\sqrt{6}}[2\alpha_{33} - \alpha_{22} - \alpha_{11}]$. Assuming a linearly polarized external field $\boldsymbol{\varepsilon}^{\mathrm{LF}} = (0,0,\varepsilon)$ and exploiting the fact that in the spherical representation the transformation between the LF and BF frames can be realized by Wigner matrices [53], the interaction term can be written as

$$\begin{aligned}\boldsymbol{\varepsilon}^{\mathrm{LF}}(\boldsymbol{\alpha}^{\mathrm{LF}}\boldsymbol{\varepsilon}^{\mathrm{LF}}) &= \varepsilon^2 \alpha_{33}^{\mathrm{LF}} = \varepsilon^2 \frac{\sqrt{6}}{3}\left(\alpha^{\mathrm{LF},(2,0)} - \frac{1}{\sqrt{2}}\alpha^{\mathrm{LF},(0)}\right) \\ &= \varepsilon^2 \frac{\sqrt{6}}{3}\left[\sum_{k=-2}^{2} D_{0k}^{2\,*}(\varphi,\vartheta,\chi)\alpha^{\mathrm{BF},(2,k)} - \frac{1}{\sqrt{2}}\alpha^{\mathrm{BF},(0)}\right]. \end{aligned} \quad \text{(A3)}$$

By recalling the well-known integral formula of the Wigner matrices [53]

$$\begin{aligned}&\int D_{M_1' M_1}^{J_1}(R) D_{M_2' M_2}^{J_2}(R) D_{M_3' M_3}^{J_3}(R) dR \\ &\quad = 8\pi^2 \begin{pmatrix} J_1 & J_2 & J_3 \\ M_1' & M_2' & M_3' \end{pmatrix}\begin{pmatrix} J_1 & J_2 & J_3 \\ M_1 & M_2 & M_3 \end{pmatrix}, \end{aligned} \quad \text{(A4)}$$

where R represents some parametrization of the SO(3) rotation group, such as the three Euler angles, and $\left(\begin{smallmatrix} J_1 & J_2 & J_3 \\ M_1 & M_2 & M_3 \end{smallmatrix}\right)$ are $3j$ symbols, the matrix elements of the complete Hamiltonian of Eq. (A1) can be expressed as

$$\begin{aligned}\langle \Psi^{JMn}|\hat{H}|\Psi^{J'M'n'}\rangle &= E^{Jn}\delta_{JJ'}\delta_{nn'}\delta_{MM'} - \frac{\varepsilon(t)^2}{2\sqrt{6}}\left[\sum_{k=-2}^{2}\langle \Psi^{JMn}\left|D_{0k}^{2\,*}\alpha^{\mathrm{BF},(2,k)}\right|\Psi^{J'M'n'}\rangle - \frac{1}{\sqrt{2}}\langle \Psi^{JMn}|\alpha^{\mathrm{BF},(0)}|\Psi^{J'M'n'}\rangle\right], \\ &= E^{Jn}\delta_{JJ'}\delta_{nn'}\delta_{MM'} \\ &\quad - \delta_{MM'}\frac{\varepsilon^2(t)}{2\sqrt{6}}\sum_{k=-2}^{2}\left[\sum_{v,v'}\langle v|\alpha^{\mathrm{BF},(2,k)}|v'\rangle \sum_{K,K'} C_{Kv}^{Jn*} C_{K'v'}^{J'n'}(2J+1)^{\frac{1}{2}}(2J'+1)^{\frac{1}{2}}(-1)^{-k+M-K'}\right. \\ &\quad \left.\times \begin{pmatrix} J & 2 & J' \\ M & 0 & -M \end{pmatrix}\begin{pmatrix} J & 2 & J' \\ K & -k & -K' \end{pmatrix}\right] + \delta_{JJ'}\delta_{MM'}\frac{\varepsilon^2(t)}{2\sqrt{12}}\sum_{v,v'}\sum_{K} C_{Kv}^{Jn*} C_{Kv'}^{J'n'}\langle v|\alpha^{\mathrm{BF},(0)}|v'\rangle, \end{aligned} \quad \text{(A5)}$$

where E^{Jn} are the field-free eigenenergies of the system and $|v\rangle$ corresponds to the vibrational basis function $\psi_v(R,r,\theta)$. To allow for the accurate evaluation of the polarizability matrix elements $\langle v|\alpha^{\mathrm{BF}}|v'\rangle \equiv \int_0^\pi \int_0^\infty \int_0^\infty \psi_v^*(R,r,\theta)\alpha^{\mathrm{BF}}(R,r,\theta)\psi_{v'}(R,r,\theta)\sin(\theta) dR dr d\theta$, the α^{BF} polarizability surfaces of H_2He^+ were constructed by

interpolation on a uniform grid of 11900 single point calculations carried out with GAUSSIAN [54] on a CCSD/aug-cc-pVTZ level [34,35,36].

After diagonalizing the Hamiltonian of Eq. (A1), physical quantities corresponding to the aligned states were evaluated by taking their expectation values with the eigenvectors of the Hamiltonian. Since the eigenvectors corresponding to the aligned states are expanded in the field-free rovibrational eigenstates, the matrix representation of the respective physical quantities in the basis of the field-free states were computed beforehand. Based on the expansion of Eq. (A2), the matrix elements of a $f(R,r,\theta)$ general function of the internal coordinates can be written as

$$\langle \Psi^{JMn}|f(R,r,\theta)|\Psi^{J'M'n'}\rangle = \delta_{JJ'}\delta_{MM'}\sum_{v,v'}\sum_{K} C_{Kv}^{Jn*}C_{Kv'}^{J'n'}\langle v|f(R,r,\theta)|v'\rangle, \quad \text{(A6)}$$

while for the ϕ angle between the z axes of the body-fixed and laboratory-fixed coordinate frames, the matrix elements of $\cos^2\phi$ can be written as [55]

$$\langle \Psi^{JMn}|\cos^2\phi|\Psi^{J'M'n'}\rangle = \sum_{v}\sum_{K,K'} C_{Kv}^{Jn*}C_{K'v}^{J'n'}\left[\frac{1}{3}\delta_{JJ'}\delta_{KK'}\delta_{MM'} + \frac{2}{3}(2J+1)^{\frac{1}{2}}(2J'+1)^{\frac{1}{2}}(-1)^{M'+K'} \times \begin{pmatrix} J & 2 & J' \\ M & 0 & -M' \end{pmatrix}\begin{pmatrix} J & 2 & J' \\ K & 0 & -K' \end{pmatrix}\right]. \quad \text{(A7)}$$

APPENDIX B: ABSORBING BOUNDARY CONDITION (ABC) TIME PROPAGATOR

Time propagation of the nuclear wave packet was done using the so-called ABC time propagator introduced in Ref. [42], which can be written as

$$\hat{U}(t) = \sum_{n=0} a_n(t)Q_n(\hat{H}_{\text{norm}}(t);\hat{\gamma}), \quad \text{(B1)}$$

where the time-dependent coefficients are the same as those for the conventional Chebyshev expansion of the unitary time propagator [56]

$$a_n(t) = (2-\delta_{n0})e^{-i\bar{H}t}(-i)^n J_n(\Delta H t), \quad \text{(B2)}$$

and the operators $Q_n(\hat{H}_{\text{norm}}(t);\hat{\gamma})$ satisfy the modified Chebyshev recursion relations

$$Q_{n+1} = 2e^{-\hat{\gamma}}\hat{H}_{\text{norm}}(t)\,Q_n - e^{-2\hat{\gamma}}Q_{n-1}, \qquad Q_0 = \hat{I},$$
$$Q_1 = \hat{H}_{\text{norm}}(t). \quad \text{(B3)}$$

In the above equations $\hat{H}_{\text{norm}}(t) = [\hat{\mathbf{H}}^{\text{2D,Jacobi}}(t) - \bar{H}]/\Delta H$, $\bar{H} = (H_{\max} + H_{\min})/2$, $\Delta H = (H_{\max} - H_{\min})/2$, $H_{\max}$ and $H_{\min}$ were chosen to be the largest and smallest eigenvalues of $\hat{\mathbf{H}}^{\text{2D,Jacobi}}(t=0)$, respectively. J_n is the nth Bessel function of the first kind [57], and $\hat{\gamma}$ is an operator which should be nonzero in the coordinate regions where wave-packet absorption is required. In the current work, following careful and extensive testing, the choice of

$$\hat{\gamma}(R,r) = \hat{\gamma}^{10}(R)\hat{\gamma}^{15}(r) \quad \text{(B4)}$$

was made, where R and r are the stretching-type Jacobi coordinates and

$$\hat{\gamma}^a(x) = \begin{cases} 0.1(e^{\left(\frac{x-a}{x_{\max}-a}\right)}-1), & \text{if } x > a \\ 0, & \text{otherwise.} \end{cases} \quad \text{(B5)}$$

Because using DVR-type basis sets has an advantage that all coordinate operators have a diagonal matrix representation, $\hat{\gamma}(R,r)$ is also diagonal and can be exponentiated straightforwardly when applying Eq. (B3).

[1] A. D. Bandrauk, *Molecules in Laser Fields* (Marcel Dekker, New York, 1994).
[2] O. Atabek, R. Lefebvre, and T. T. Nguyen-Dang, Adv. Quantum Chem. **60**, 51 (2010).
[3] K. Sändig, H. Figger, and T.W. Hänsch, Phys. Rev. Lett. **85**, 4876 (2000).
[4] P.H. Bucksbaum, A. Zavriyev, H. G. Muller, and D. W. Schumacher, Phys. Rev. Lett. **64**, 1883 (1990).
[5] A. Giusti-Suzor, X. He, O. Atabek, and F. H. Mies, Phys. Rev. Lett. **64**, 515 (1990).
[6] G. J. Halász, A. Csehi, Á. Vibók, and L. S. Cederbaum, J. Phys. Chem. A **118**, 11908 (2014).
[7] I. Maruyama, T. Sako, and K. Yamanouchi, J. Phys. B: At. Mol. Opt. Phys. **37**, 3919 (2004).
[8] T. Abel, P. Anninos, Y. Zhang, and M. L. Norman, N. Astron. **2**, 181 (1997).
[9] E. Herbst, Ann. Rev. Phys. Chem. **46**, 27 (1995).
[10] K. M. Ferrière, Rev. Mod. Phys. **73**, 1031 (2001).
[11] S. Lepp, P. C. Stancil, and A. Dalgarno, J. Phys. B: At., Mol. Opt. Phys. **35**, R57 (2002).
[12] D. De Fazio, Phys. Chem. Chem. Phys. **16**, 11662 (2014), and references therein.
[13] E. Herbst, Philos. Trans. R. Soc., A **358**, 2523 (2000).
[14] J. Tennyson and S. Miller, J. Chem. Phys. **87**, 6648 (1987).
[15] L. Page and D. Wilkinson, Rev. Mod. Phys. **71**, S173 (1999).
[16] B. A. Remington, R. P. Drake, and D. D. Ryutov, Rev. Mod. Phys. **78**, 755 (2006); see Sec. IX and references therein.
[17] M.-H. Ulrich, L. Maraschi, and C. M. Urry, Annu. Rev. Astron. Astrophys. **35**, 445 (1997).
[18] R. Johnsen, A. Chen, and M. A. Biondi, J. Chem. Phys. **72**, 3085 (1980).

[19] J. E. Pollard, J. A. Syage, L. K. Johnson, and R. B. Cohen, J. Chem. Phys. **94**, 8615 (1991).
[20] E. G. Jones, L. C. Wu, B. M. Hughes, T. O. Tiernan, and D. G. Hopper, J. Chem. Phys. **73**, 5631 (1980).
[21] A. Carrington, D. I. Gammie, A. M. Shaw, S. M. Taylor, and J. M. Hutson, Chem. Phys. Lett. **260**, 395 (1996).
[22] V. Špirko and W. P. Kraemer, J. Mol. Spectrosc. **172**, 265 (1995).
[23] C. N. Ramachandran, D. De Fazio, S. Cavalli, F. Tarantelli, and V. Aquilanti, Chem. Phys. Lett. **469**, 26 (2009).
[24] P. Palmieri, C. Puzzarini, V. Aquilanti, G. Capecchi, S. Cavalli, D. DeFazio, A. Aguilar, X. Giménez, and J. M. Lucas, Mol. Phys. **98**, 1835 (2000).
[25] D. De Fazio, M. de Castro-Vitores, A. Aguado, V. Aquilanti, and S. Cavalli, J. Chem. Phys. **137**, 244306 (2012).
[26] W. P. Kraemer, V. Špirko, and O. Bludskŷ, Chem. Phys. **276**, 225 (2002).
[27] A. Aguado, C. Suárez, and M. Paniagua, J. Chem. Phys. **98**, 308 (1993).
[28] V. Sidis, Chem. Phys. **209**, 313 (1996).
[29] M. Juřek, V. Špirko, and W. P. Kraemer, J. Mol. Spectrosc. **182**, 364 (1997).
[30] M. Šindelka, V. Špirko, and W. P. Kraemer, Theor. Chem. Acc. **110**, 170 (2003).
[31] F. Mrugała and W. P. Kraemer, J. Chem. Phys. **122**, 224321 (2005).
[32] F. Mrugała and W. P. Kraemer, J. Chem. Phys. **138**, 104315 (2013).
[33] C. G. J. Jacobi, C. R. Hebd. Seances Acad. Sci. **15**, 236 (1842).
[34] R. J. Bartlett, C. E. Dykstra, and J. Paldus, *Advanced Theories and Computational Approaches to the Electronic Structure of Molecules* (Reidel, Dordrecht, 1984).
[35] T. H. Dunning, Jr., J. Chem. Phys. **90**, 1007 (1989).
[36] R. A. Kendall, T. H. Dunning, Jr., and R. J. Harrison, J. Chem. Phys. **96**, 6796 (1992).
[37] MRCC, a quantum chemical program suite written by M. Kállay, Z. Rolik, J. Csontos, I. Ladjánszki, L. Szegedy, B. Ladóczki, and G. Samu; see also Z. Rolik, L. Szegedy, I. Ladjánszki, B. Ladóczki, and M. Kállay, J. Chem. Phys. **139**, 094105 (2013), as well as http://www.mrcc.hu.
[38] G. A. Worth and L. S. Cederbaum, Annu. Rev. Phys. Chem. **55**, 127 (2004).
[39] H.-J. Werner and W. Meyer, J. Chem. Phys. **74**, 5802 (1981).
[40] C. Fábri, E. Mátyus, and A. G. Császár, J. Chem. Phys. **134**, 074105 (2011).
[41] J. C. Light and T. Carrington, Adv. Chem. Phys. **114**, 263 (2000).
[42] V. A. Mandelshtam and H. S. Taylor, J. Chem. Phys. **103**, 2903 (1995).
[43] C.-W. Lee and Y. Gim, J. Phys. B: At. Mol. Opt. Phys. **46**, 215001 (2013).
[44] See, for example, V. Ryaboy, N. Moiseyev, V. A. Mandelshtam, and H. S. Taylor, J. Chem. Phys. **101**, 5677 (1994); B. Poirier and T. Carrington, Jr., *ibid.* **116**, 1215 (2002); B. C. Silva, P. Barletta, J. J. Munro, and J. Tennyson, *ibid.* **128**, 244312 (2008).
[45] F. Riesz and B. Sz-Nagy, *Functional Analysis* (Ungar, New York, 1955).
[46] B. Friedrich and D. Herschbach, Phys. Rev. Lett. **74**, 4623 (1995).
[47] T. Szidarovszky, A. G. Császár, and G. Czakó, Phys. Chem. Chem. Phys. **12**, 8373 (2010).
[48] C. M. Dion, A. D. Bandrauk, O. Atabek, A. Keller, H. Umeda, and Y. Fujimura, Chem. Phys. Lett. **302**, 215 (1999).
[49] S. Hervé, F. Le Quéré, and R. Marquardt, J. Chem. Phys. **116**, 3300 (2002).
[50] J. Floß, T. Grohmann, M. Leibscher, and T. Seideman, J. Chem. Phys. **136**, 084309 (2012).
[51] P. R. Bunker and P. Jensen, *Molecular Symmetry and Spectroscopy* (NRC Research Press, Ottawa, Canada, 1998).
[52] T. Szidarovszky and A. G. Császár, Mol. Phys. (Martin Quack Special Issue) **111**, 2131 (2013).
[53] R. N. Zare, *Angular Momentum* (Wiley, New York, 1988).
[54] M. J. Frisch, G. W. Trucks, H. B. Schlegel, G. E. Scuseria, M. A. Robb, J. R. Cheeseman, G. Scalmani, V. Barone, B. Mennucci, G. A. Petersson, H. Nakatsuji, M. Caricato, X. Li, H. P. Hratchian, A. F. Izmaylov, J. Bloino, G. Zheng, J. L. Sonnenberg, M. Hada, M. Ehara *et al.*, Gaussian, Inc., Wallingford, CT, 2009.
[55] V. Makhija, X. Ren, and V. Kumarappan, Phys. Rev. A **85**, 033425 (2012).
[56] H. Tal-Ezer and R. Kosloff, J. Chem. Phys. **81**, 3967 (1984).
[57] M. Abramowitz and I. A. Stegun, *Handbook of Mathematical Functions with Formulas, Graphs, and Mathematical Tables*, 9th printing (Dover, New York, 1972).